INTERNATIONAL JOURNAL FOR NUMERICAL METHODS IN FLUIDS
Int. J. Numer. Meth. Fluids 2003; **42**:1211–1236 (DOI: 10.1002/fld.586)

Modified method of characteristics for solving population balance equations

Laurent Pilon[1,*,†] and Raymond Viskanta[2]

[1] *Mechanical and Aerospace Engineering Department, University of California, Los Angeles, U.S.A.*
[2] *School of Mechanical Engineering, Purdue University-West Lafayette, U.S.A.*

SUMMARY

This paper presents a new numerical method for solving the population balance equation using the modified method of characteristics. Aggregation and break-up are neglected but the density function variations in the three-dimensional space and its dependence on the external fields are accounted for. The method is an interpretation of the Lagrangian approach. Based on a pre-specified grid, it follows the particles backward in time as opposed to forward in the case of traditional method of characteristics. Unlike the direct marching method, the inverse marching method uses a fixed grid thus, making it compatible with other numerical schemes (e.g. finite-volume, finite elements) that may be used to solve other coupled equations such as the mass, momentum, and energy conservation equations. The numerical solutions are compared with the exact analytical solutions for simple one-dimensional flow cases. Very good agreement between the numerical and the theoretical solutions has been obtained confirming the validity of the numerical procedure and the associated computer program. Copyright © 2003 John Wiley & Sons, Ltd.

KEY WORDS: population balance theory; method of characteristics; dispersed phases; particulate flows; two-phase flow

1. INTRODUCTION

Physical modelling of multidimensional particulate flows has been the subject of intense research over the last half century. The two-fluid model is often considered as the most sophisticated multidimensional models available in the literature [1, 2]. In three-dimensional gas/liquid flows, the two-fluid model is comprised of 10 scalar partial differential equations, five scalar algebraic interfacial jump conditions and eleven state variables. However, as reviewed by Lahey and Drew [2] while the rigorous derivation of the two-fluid models has made significant progresses, 'no model exists to date which is completely acceptable'. Moreover, mechanistic interfacial and wall closure laws are still needed to accurately model three-dimensional two-phase flow [2]. More recently, Carrica *et al.* [3] have presented a three-dimensional com-

* Correspondence to: L. Pilon, Henri Samueli School of Engineering and Applied Science, University of California at Los Angeles, 420 Westwood Plaza, 37-132 Engineering IV, Los Angeles, CA 90095, U.S.A.
† E-mail: pilon@seas.ucla.edu

Received 10 December 2002
Revised 22 April 2003

putational model for two-phase flow around a naval surface ship. The formulation is based on a multidimensional two-fluid model [2] consisting of the continuity and the momentum equations for both the gas and the liquid phases combined with the conservation equation for the total number of bubbles. The numerical algorithm is based on a finite-difference method and can calculate the gas volume fraction and bubble radius and accounts for the coupling between the gas and the liquid equations. However, it is limited to monodispersed bubble population, i.e. all the bubbles at each location have the same radius. This was recognized as an obvious limitation [2]. Such limitation could be overcome by solving the bubble population balance equation for a polydisperse bubble density function.

Indeed, population balance offers a framework to solve various dispersed phase systems with applications ranging from crystallization and fluidized bed reactors to microbial cultures and aerosol reactors. As discussed in detail by Ramkrishna [4, 5], the particle population can be described by a state vector defined in a so-called state space. The state space consists not only of the physical space but also of an abstract 'property' space. In the physical space, the state vector co-ordinates consist of the spatial co-ordinates [e.g. (x, y, z) in Cartesian co-ordinates]. In the property space, the system is characterized by its property co-ordinates. For example, each particle is characterized by its radius r and other properties denoted p_i such as gas molar fractions inside the bubbles in the case of gas/liquid flows. The spatial and property co-ordinates are also referred to as the external and internal co-ordinates, respectively. Considering the particles transported by the liquid flow and characterized by their radius r and l other properties p_i the state vector $\mathbf{S}$ can be expressed as $\mathbf{S} = [x, y, z, t, r, (p_i)_{1 \leqslant i \leqslant l}]$. Let f_1 be the average number density function of particles/bubbles. The average number density function $f_1[\mathbf{x}, t, r, (p_i)_{1 \leqslant i \leqslant l}]$ is assumed to be sufficiently smooth to allow differentiation with respect to any of its variables as many times as necessary [5]. Then, the population balance equation can be expressed as [5]

$$\frac{\partial f_1}{\partial t} + \frac{\partial}{\partial x}(u_b f_1) + \frac{\partial}{\partial y}(v_b f_1) + \frac{\partial}{\partial z}(w_b f_1) + \frac{\partial}{\partial r}(\dot{r} f_1) + \sum_{i=1}^{l} \frac{\partial}{\partial p_i}(\dot{p}_i f_1) = h \tag{1}$$

where u_b, v_b and w_b are the components of the particle velocity vector $\mathbf{v}_b$. The time rate of change of the radius and of the other properties of the particles are denoted by $\dot{r}$ and $\dot{p}_i$, respectively. Finally, $h = h(\mathbf{x}, t, r, p_i, Y_i)$ represents the net rate of production of particles of a particular state $(\mathbf{x}, r, (p_i)_{1 \leqslant i \leqslant l})$ at time t.

Three levels of complexity arise in solving the population balance equation: (1) the source and sink terms resulting from breakage and agglomeration and expressed as integral functions in the population balance equation, (2) the variation of the density function in the multidimensional space, and (3) the dependency of the density function on external variables Y_i. Reference is deliberately made to papers dealing only with density function depending on the three dimensions and on external variables. The numerous publications in which spatial variation of the density functions was neglected by assuming perfectly mixed tank (e.g. References [6–9]) are not discussed. However, the method can be extended to situations where the sink and the source are present. In these cases, comparison with numerical solution is required but falls beyond the scope of the present study.

Both analytical and numerical methods for solving the population balance equation have been recently reviewed by Ramkrishna [5]. For the most practical problems, numerical methods are required if one wants to avoid simplistic assumptions. Discretization of the density function combined with finite difference method has been one of the most popular numerical

methods [5, 10–13]. It consists of discretizing the particle density function in the internal space, thus forming groups of particles and solving the resulting equations for the total number of particles in each group by a finite-difference method. Such a method has the advantage of reducing computational times, a valuable feature in control and optimization of particulate systems [5]. However, the discrete formulation has major drawbacks that have been discussed extensively by Kumar and Ramkrishna [7, 9]. In brief, the discrete formulation lacks of *internal consistency*, i.e. some of the moments of the particle density function f_1 cannot be predicted accurately. For example, in gas/liquid flows in which bubbles are characterized by their radius r at time t, the mth sectional and total moments of the bubble density function f_1 in terms of bubble radius, denoted by $\mu_m^{(i)}(\mathbf{x},t)$ and $\mu_m(\mathbf{x},t)$, respectively, are defined as

$$\mu_m^{(i)}(\mathbf{x},t)=\int_{r_i}^{r_{i+1}} r^m f_1(\mathbf{x},r,t)\,\mathrm{d}r \quad \text{and} \quad \mu_m(\mathbf{x},t)=\int_{r_0}^{r_N} r^m f_1(\mathbf{x},r,t)\,\mathrm{d}r=\sum_{i=0}^{N-1}\mu_m^{(i)}(t) \tag{2}$$

where r_0 and r_N are the minimum and maximum bubble radius. The total number of particles, the average particle radius, the interfacial area concentration, the local volume fraction of the dispersed phase are essential physically important moments of the particle density function and correspond to zero, first, second and third order moments in terms of the particle radius, respectively. For bubbles containing a single gas or a diffusing and a non-diffusing gas, the bubble radius r is treated as the independent internal variable and N, A_i, f_v and $\bar{r}$ are defined, respectively, as

$$\text{zeroth moment} \quad N(x,y,z)=\int_0^\infty f_1(x,y,z,r)\,\mathrm{d}r \tag{3}$$

$$\text{First moment} \quad \bar{r}(x,y,z)=\left[\int_0^\infty r f_1(x,y,z,r)\,\mathrm{d}r\right]\Big/ N(x,y,z) \tag{4}$$

$$\text{Second moment} \quad A_i(x,y,z)=\int_0^\infty 4\pi r^2 f_1(x,y,z,r)\,\mathrm{d}r \tag{5}$$

$$\text{Third moment} \quad f_v(x,y,z)=\int_0^\infty \frac{4\pi r^3}{3} f_1(x,y,z,r)\,\mathrm{d}r \tag{6}$$

Another important moment in gas/liquid flows is the total mass of gas contained in the bubbles defined as the third order moment in terms of variable $4\pi r^3\rho_g/3$. In the discretization technique, the calculation is designed for certain selected moments of the particle density function rather than for an estimate of the particle density function accurate enough for estimating *all* moments of the population [5]. In addition to the total number of particles/bubbles for each discrete group, the discretized formulation for the second and third order moments should also be solved if one wants to accurately predict (1) the interfacial mass and momentum transfer between the phases [1, 2], (2) the flow regime often determined from the void fraction and (3) the corresponding closure laws [1]. For example, Rousseaux *et al.* [12] solved the coupled conservation equations for the total zeroth to fourth moments of the density function of pseudo-boehmite particles accounting for growth and precipitation in sliding surface mixing devices. However, this approach does not provide detailed information about the density function unless one assumes an arbitrary prespecified form with four unknown parameters such as the modified Gamma distribution.

The method of characteristics offers an alternative and more accurate method to discretization method combined with finite-difference methods. Instead of creating groups of particles/bubbles, it solves directly for f_1 and consists of transforming the partial differential population balance equation into a system of ordinary differential equation which is then solved along the pathline of the particles (characteristic curves). The conventional implementation (or *direct marching method*) of the method of characteristics is based on the Lagrangian formulation: the particles or the particle density function are identified and located at initial time $t = t_0$ and followed at subsequent time as the particles are transported. In three-dimensional flows, however, the deformation that the initial mesh undergoes as time progresses might lead to deterioration of the numerical solution [14].

The modified method of characteristics (or *inverse marching method*) is an intepretation of the Lagrangian approach that overcomes the difficulties related to mesh deformation [14]. Based on a pre-specified grid, it follows the particles backward in time as opposed to forward, in the case of direct marching method. Unlike the direct marching method, the inverse marching method uses a fixed grid that can be used for solving other transport equations such as the continuity, momentum and energy equations by finite-difference methods using a staggered grid, as suggested by Patankar [15]. The advantages of the modified method of characteristics are the following:

- unlike finite-difference methods in which the information propagates along co-ordinate lines, the method of characteristics propagates the information along the pathlines and thus matches the physics of the flow resulting in extremely accurate numerical results [16].
- it overcomes the numerical diffusion introduced by finite-difference methods [15].
- it does not require any outflow boundary conditions [17].
- Since the method uses a pre-specified computational grid, it can easily account for the coupling between the density function f_1 and the external fields such as the temperature, velocity and concentrations which can be obtained by other numerical methods based on an Eulerian field description (e.g. finite volume method [15]).
- The modified method of characteristics can be used for both transient and steady-state calculations with great accuracy and without problems of numerical instability.

However, it possesses significant, although not overwhelming, disadvantages [16]: (1) it is a relatively complicated procedure, especially for more than three or four independent variables, (2) the method is restricted to flows and variables without discontinuities and (3) due to the large amount of required interpolations and integration of the governing ordinary differential equations, the computer programs may require long execution times.

The modified method of characteristics has been successfully used for predicting high speed three-dimensional single phase inviscid flows in subsonic and supersonic propulsion nozzles [16–19] and combined with finite elements method for solving unsteady incompressible Navier–Stokes equations [14]. On the other hand, the conventional method of characteristics for solving the population balance equation has been mainly used (1) for mathematical arguments to show the existence of solutions [5], (2) for obtaining analytical solutions [5, 20–22] and (3) for obtaining numerical solution for two independent variables problems [9]. However, to the best of our knowledge, no attempt has been made to solve the population balance equation by the modified method of characteristics. As computers become more powerful and cheaper, the present approach favours accuracy and numerical stability over short

computational time and algorithm simplicity. This paper presents a numerical implementation of the modified method of characteristics for solving the population balance equation in multiphase particulate systems that could be coupled to other numerical schemes for solving the two-fluid model equations, or any other transport equations.

2. MODIFIED METHOD OF CHARACTERISTICS

The present study is concerned with solving the population balance equation for solid particle, gas bubbles, or solid droplets transported in three-dimensional flow using the modified method of characteristics. A Cartesian co-ordinate system was employed in the analysis. The formulation of the population balance equation is based on the following general assumptions that hold for many different multiphase particulate systems:

1. The particles are perfectly spherical in shape.
2. The effects of particles on the velocity and temperature fields as well as on the thermophysical properties of the liquid phase are not considered.
3. Particle radius and local concentration are small.
4. The particles have negligible inertia ($\rho_b \ll \rho_\infty$). This hypothesis is reasonable since very small particles are considered.
5. The liquid phase is incompressible.
6. Local thermal equilibrium exists between the gas and liquid phases, i.e. $T_\infty = T_b = T$.
7. Aggregation and break up of particles are not considered, i.e. the net production rate of particles vanishes ($h = 0$).
8. The components of the particle velocity vector, are taken to be the same as those of the liquid phase $\mathbf{v}_\infty = (u_\infty, v_\infty, w_\infty)$, except in the vertical direction where the buoyancy force has to be taken into account, i.e.

$$\mathbf{v_b}(r) = u_\infty \mathbf{i} + v_\infty \mathbf{j} + (w_\infty + w_r)\mathbf{k} \tag{7}$$

with w_r being the upward particle velocity relative to the liquid phase due to the buoyancy force and is assumed to follow Stokes' law, i.e.

$$w_r = \frac{2}{9}\frac{\rho_\infty g r^2}{\mu_\infty} \tag{8}$$

Note that Equation (8) corresponds to the terminal (i.e. steady state) velocity of spherical particles in Stokes' flow, i.e. the transient motion and inertia of particles have not been considered for the sake of simplicity and since the formulation of transient forces is still incomplete [23].

Based on the above assumptions, the population balance equation simplifies to

$$\frac{\partial f_1}{\partial t} + \frac{\partial}{\partial x}(u_\infty f_1) + \frac{\partial}{\partial y}(v_\infty f_1) + \frac{\partial}{\partial z}[(w_\infty + w_r) f_1] + \frac{\partial}{\partial r}(\dot{r} f_1) + \sum_{i=1}^{l} \frac{\partial}{\partial p_i}(\dot{p}_i f_1) = 0 \tag{9}$$

The method of characteristics consists of solving the population balance equation along the pathline of the particles and transforms the governing partial differential equation into a system of ordinary differential equations.

If we assume that the liquid phase can be treated as incompressible, the mass conservation equation for the liquid phase can be expressed as [24]

$$\nabla \cdot \mathbf{v}_\infty = \frac{\partial u_\infty}{\partial x} + \frac{\partial v_\infty}{\partial y} + \frac{\partial w_\infty}{\partial z} = 0 \tag{10}$$

Expanding the partial derivatives on the left-hand side of Equation (1) and using Equation (10) yields

$$\frac{\partial f_1}{\partial t} + u_\infty \frac{\partial f_1}{\partial x} + v_\infty \frac{\partial f_1}{\partial y} + w_\infty \frac{\partial f_1}{\partial z} + \dot{r}\frac{\partial f_1}{\partial r} + \sum_{i=1}^{l} \dot{p}_i \frac{\partial f_1}{\partial p_i} = -f_1 \left[\frac{\partial w_r}{\partial z} + \frac{\partial \dot{r}}{\partial r} + \sum_{i=1}^{l} \frac{\partial \dot{p}_i}{\partial p_i} \right] \tag{11}$$

By definition, the total time derivative of $f_1 = f_1[x, y, z, t, r, (p_i)_{1 \leqslant i \leqslant l}]$ with respect to time t can be written as

$$\frac{\mathrm{d}f_1}{\mathrm{d}t} = \frac{\partial f_1}{\partial t} + \frac{\mathrm{d}x}{\mathrm{d}t}\frac{\partial f_1}{\partial x} + \frac{\mathrm{d}y}{\mathrm{d}t}\frac{\partial f_1}{\partial y} + \frac{\mathrm{d}z}{\mathrm{d}t}\frac{\partial f_1}{\partial z} + \frac{\mathrm{d}r}{\mathrm{d}t}\frac{\partial f_1}{\partial r} + \sum_{i=1}^{l} \frac{\mathrm{d}p_i}{\mathrm{d}t}\frac{\partial f_1}{\partial p_i} \tag{12}$$

We further define the characteristic curves in the particle state space as

$$\frac{\mathrm{d}x}{\mathrm{d}t} = u_\infty(x, y, z) \tag{13}$$

$$\frac{\mathrm{d}y}{\mathrm{d}t} = v_\infty(x, y, z) \tag{14}$$

$$\frac{\mathrm{d}z}{\mathrm{d}t} = w_\infty(x, y, z) + w_r(x, y, z, r) \tag{15}$$

$$\frac{\mathrm{d}r}{\mathrm{d}t} = \dot{r}[x, y, z, r, (p_i)_{1 \leqslant i \leqslant l}, (Y_j)_{1 \leqslant j \leqslant l}, t] \tag{16}$$

$$\frac{\mathrm{d}p_i}{\mathrm{d}t} = \dot{p}_i[x, y, z, r, (p_i)_{1 \leqslant i \leqslant l}, (Y_j)_{1 \leqslant j \leqslant l}, t] \quad \text{for } i = 1, \ldots, l \tag{17}$$

where $(Y_j)_{1 \leqslant j \leqslant l}$ are the local continuous phase variables e.g. the gas concentration dissolved in the liquid phase, the liquid temperature, or velocity. These variables are introduced to consider the coupling between the density function f_1 and the external fields. Then, along the characteristic curves in the $[x, y, z, r, (p_i)_{1 \leqslant i \leqslant l}, t]$ space, the population balance equation can be written as

$$\frac{\mathrm{D}f_1}{\mathrm{D}t} = -f_1 \left[\frac{\partial w_r}{\partial z} + \frac{\partial \dot{r}}{\partial r} + \sum_{i=1}^{l} \frac{\partial \dot{p}_i}{\partial p_i} \right] \tag{18}$$

where $\mathrm{D}f_1/\mathrm{D}t$ denotes the substantial derivative of f_1, i.e. the total time derivative along the pathline of the particle. The partial derivative of w_r with respect to z is obtained from

Equation (8) and is expressed as

$$\frac{\partial w_r}{\partial z} = \frac{4\rho_\infty g r \dot{r}}{9\mu_\infty (w_\infty + w_r)} \tag{19}$$

Similarly, expressions for $\dot{r}$ and $\dot{p}_i$ and their derivatives with respect to r and p_i, respectively, can be obtained based on physical considerations of the specific process to be modelled.

In the method of characteristics, no boundary condition is required at the outflow [17] while the particle density function is specified at the inlet boundary (x_0, y_0, z_0)

$$f_1(x_0, y_0, z_0, t) = f_{1,0}[r, (p_i)_{1 \leqslant i \leqslant l}, t] \tag{20}$$

At the container wall/liquid interface the gradient of the particle density function f_1 in the normal direction vanishes,

$$\nabla_{\mathbf{n}} f_1 = \mathbf{0} \quad \text{at the liquid/walls interface} \tag{21}$$

Assumptions regarding the bubble velocity and neglect of the effects of particles on the liquid phase flow and temperature fields are the most severe ones and their limitations will be discussed later in this document. They have been used to decouple the conservation, momentum and energy equations of the liquid and gas phases. This approach can be justified by the facts that particle radius and concentration are small and that the alternative approach solving the coupled governing equations using the multidimensional two-fluid model lacks mechanistic closure laws accounting, for example, for the interfacial mass and momentum transfer [2].

3. NUMERICAL METHOD

In the present model, the liquid flow is assumed not to be affected by the presence of particles; therefore, the velocity and temperature fields in the liquid phase are treated as fixed input parameters. The system of equations for the velocity and temperature fields are parabolic in nature and can be discretized in space using a $(l_1 \times m_1 \times n_1)$ staggered grid for the scalar and vector variables and can be solved, for example, by using the SIMPLER algorithm [15]. Indices i, j, k correspond to the vector grid points while indices I, J, K correspond to the scalar grid points as illustrated in Figures 1 and 2 for two-dimensional geometry. Other external variables related to the liquid phase, such as the dissolved gas concentrations, can be computed in a similar manner.

The governing equations [Equations (13)–(21)] for the particle density function are solved by the modified method of characteristics [16, 18, 19]. Figure 3 shows a three-dimensional computational cell whose corner points belong to the vector component grid. The modified method of characteristics consists of determining the co-ordinates (x_n, y_n, z_n) of the point in space from where the particles located at the grid point (x_a, y_b, z_c) at time $t + \Delta t$ originate from at time t. In other words, for each point of a specified grid, the pathline is projected rearward to the initial data surface to determine the initial data point. For example, in Figure 3 the point (x_a, y_b, z_c) is the point $(x_{i+1}, y_{j+1}, z_{k+1})$. The solid line represents the section of the characteristic curve along which the particle traveled from location (x_n, y_n, z_n) to location (x_a, y_b, z_c) during the time interval between t and $t + \Delta t$.

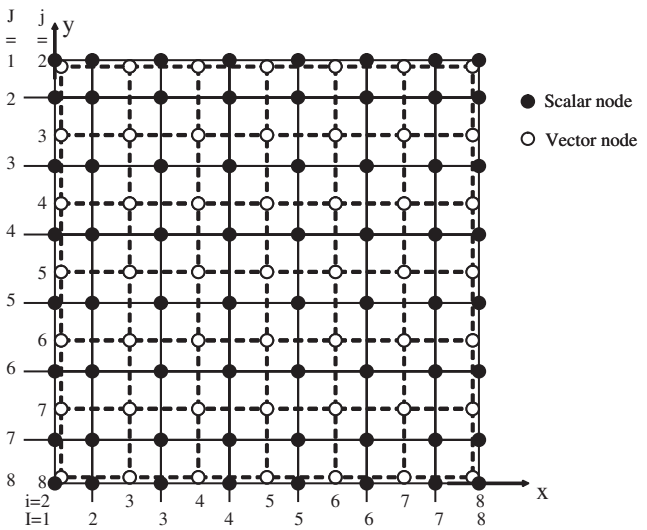

Figure 1. Schematic of a 8×8 staggered grid in a two-dimensional representative longitudinal plane ($l_1 = m_1 = 8$).

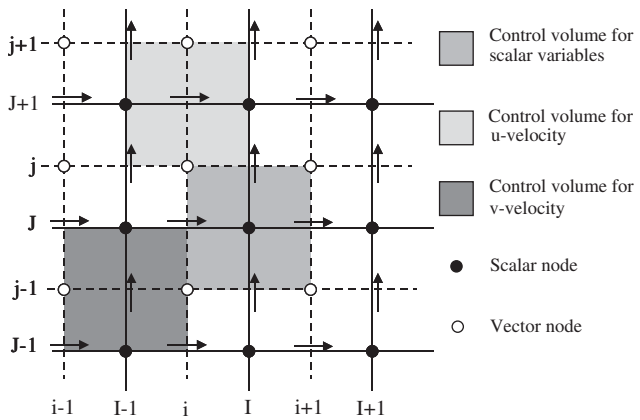

Figure 2. Definition of control volume in a two-dimensional representative longitudinal plane.

To avoid numerical instabilities, it is necessary to insure that the particles do not leave the computational cell between the time t and $t + \Delta t$. In other words, each computational cell traveled by the particle should contain at least two consecutive points on the characteristic curve. Therefore, the initial time step Δt is determined by the equation,

$$\Delta t = \min_{\substack{2 \leqslant i \leqslant l_1 - 1 \\ 2 \leqslant j \leqslant m_1 - 1 \\ 2 \leqslant k \leqslant n_1 - 1}} \left\{ \left| \frac{x_{i+1} - x_i}{2u_\infty(i,j,k)} \right|, \left| \frac{y_{j+1} - y_j}{2v_\infty(i,j,k)} \right|, \left| \frac{z_{k+1} - z_k}{2[w_\infty(i,j,k) + w_r(i,j,k)]} \right| \right\} \tag{22}$$

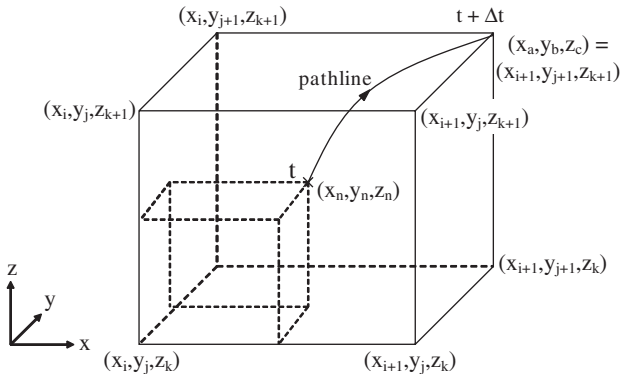

Figure 3. Typical computational cell used for inverse marching method containing the pathline of the bubbles.

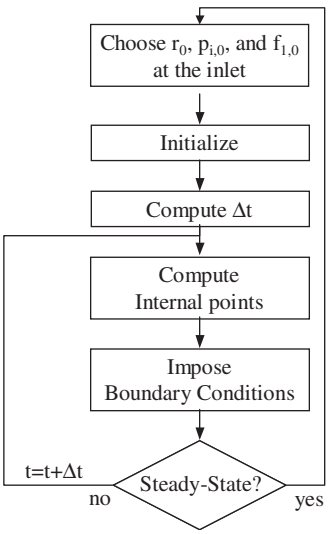

Figure 4. Block diagram of the numerical procedure for solving the population balance equation by the method of characteristics using inverse marching method.

The factor 2 appearing in the denominator was arbitrarily introduced to assure that each computational cell contains at least two consecutive points on the characteristics curve. A larger value of the factor could have been chosen but was proven to have no significant effect on the final numerical results, while slowing down the convergence to steady-state. However, when particles can grow, the particle radius and upward velocity can change making the particles leave the computational cell after one time step. Then, the time step has to be reduced in order to assure the stability requirement.

Figure 4 shows the general block diagram of the computational procedure in performing a steady-state calculation for a given particle size distribution $f_{1,0}[r,(p_i)_{1\leqslant i\leqslant l},t]$ at the inlet

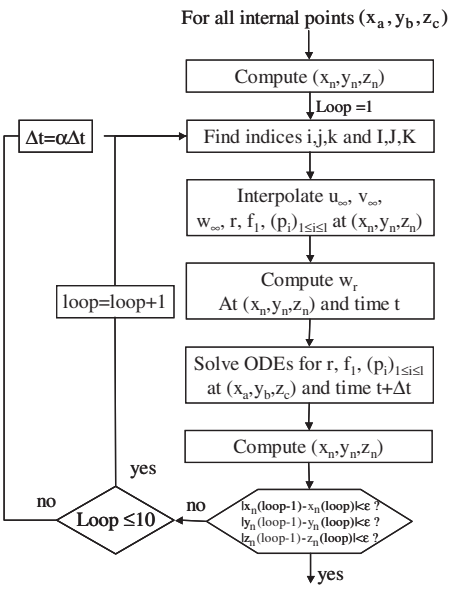

Figure 5. Block diagram of the computation of the interior point for solving the population balance equation by the method of characteristics using inverse marching method.

boundary. First, the variables across the computational domain are all initialized to an arbitrarily small value except at the inlet boundary where the variables r, $(p_i)_{1\leqslant i\leqslant l}$ and f_1 are set to be equal to r_0, $(p_{0,i})_{1\leqslant i\leqslant l}$ and $f_{1,0}$, respectively. In other words, an arbitrary point is selected on the initial particle density function $f_{1,0}[r,(p_i)_{1\leqslant i\leqslant l},t]$. Then, the time step is computed according to Equation (22). Finally, the ordinary differential equations for the variables r, $(p_i)_{1\leqslant i\leqslant l}$ and f_1 [Equations (13)–(18)] are solved at all interior points and outflow boundaries, followed by the computation of the variables at the solid boundary points. The solution of the governing ordinary differential equation at the interior points and specification of the variables at the boundaries is repeated until a steady state has been reached. The same sequence takes place for another arbitrary point with co-ordinates $[r'_0,(p'_{0,i})_{1\leqslant i\leqslant l}]$ on the initial particle density function $f_{1,0}$ imposed at the inlet boundary.

The computational domain for solving the particle density function, the particle radius and the other particle internal co-ordinates consists of four basic types of points (or nodes): interior, solid boundary, inlet and exit points. The basic features of the interior point unit process are presented in the following discussion followed by a brief description of the other three unit processes.

3.1. Interior point unit process

Figure 5 shows the detailed numerical procedure used for solving the governing ordinary differential equations [Equations (13)–(18)] at every interior point (x_a, y_b, z_c) such that $2\leqslant a\leqslant l_1-1$, $2\leqslant b\leqslant m_1-1$ and $2\leqslant c\leqslant n_1-1$ as well as at the outlet boundary.

1. First, the co-ordinates (x_n, y_n, z_n) are determined by assuming that the velocity component (u_n, v_n, w_n) and the particle radius r_n at location (x_n, y_n, z_n) and time t are the same as those at location (x_a, y_b, z_c) at time $t + \Delta t$, i.e. $(u_n, v_n, w_n) = (u_\infty, v_\infty, w_\infty + w_r)$. Thus solving Equations (13)–(15) yields

$$x_n = x_a - u_\infty(x_a, y_b, z_c)\Delta t \tag{23}$$

$$y_n = y_b - v_\infty(x_a, y_b, z_c)\Delta t \tag{24}$$

$$z_n = z_c - [w_\infty(x_a, y_b, z_c) + w_r(x_a, y_b, z_c, r)]\Delta t \tag{25}$$

2. Second, let us call (x_i, y_j, z_k) the closest point to (x_n, y_n, z_n) in the *vector* grid such that $x_i \leqslant x_n \leqslant x_{i+1},\ y_j \leqslant x_n \leqslant y_{j+1},\ z_k \leqslant x_n \leqslant z_{k+1}$. Similarly, let us call (x_I, y_J, z_K) the closest point to (x_n, y_n, z_n) in the *scalar* grid such that $x_I \leqslant x_n \leqslant x_{I+1},\ y_J \leqslant x_n \leqslant y_{J+1},\ z_K \leqslant x_n \leqslant z_{K+1}$. Then, the computational cells containing the point (x_n, y_n, z_n) in both the vector grid and the scalar grid of the staggered grid system, i.e. i, j, k and I, J, K, are determined.
3. Third, the velocity components at (x_n, y_n, z_n) are determined by Lagrangian interpolation using their values at the eight corners of the computational cell in the vector grid containing the point (x_n, y_n, z_n),

$$\begin{aligned}\phi_n = {} & (1-\beta_u)(1-\beta_v)(1-\beta_w)\phi_{i,j,k} + \beta_u(1-\beta_v)(1-\beta_w)\phi_{i+1,j,k} \\ & + (1-\beta_u)\beta_v(1-\beta_w)\phi_{i,j+1,k} + \beta_u \times \beta_v(1-\beta_w)\phi_{i+1,j+1,k} \\ & + (1-\beta_u)(1-\beta_v)\beta_w\phi_{i,j,k+1} + \beta_u(1-\beta_v)\beta_w\phi_{i+1,j,k+1} \\ & + (1-\beta_u)\beta_v \times \beta_w \times \phi_{i,j+1,k+1} + \beta_u \times \beta_v \times \beta_w \times \phi_{i+1,j+1,k+1}\end{aligned} \tag{26}$$

where the variable ϕ corresponds to the liquid velocity components u_∞, v_∞ and w_∞ and ϕ_n is their interpolated value at location (x_n, y_n, z_n), while $\phi_{i,j,k}$ is their known values at the vector grid point (x_i, y_j, z_k). The weights β_u, β_v and β_w vary between zero and unity and are defined as

$$\beta_u = \frac{(x_n - x_i)}{(x_{i+1} - x_i)}, \quad \beta_v = \frac{(y_n - y_j)}{(y_{j+1} - y_j)} \quad \text{and} \quad \beta_w = \frac{(z_n - z_k)}{(z_{k+1} - z_k)} \tag{27}$$

4. Similarly, the scalar variables ψ such as the temperature T, the radius of the particles r, the internal co-ordinate $(p_i)_{1 \leqslant i \leqslant l}$ and the thermophysical properties are interpolated at location (x_n, y_n, z_n) and time t using the equation

$$\begin{aligned}\psi_n = {} & (1-\gamma_x)(1-\gamma_y)(1-\gamma_z)\psi_{I,J,K} + \gamma_x(1-\gamma_y)(1-\gamma_z)\psi_{I+1,J,K} \\ & + (1-\gamma_x)\gamma_y(1-\gamma_z)\psi_{I,J+1,K} + \gamma_x \times \gamma_y(1-\gamma_z)\psi_{I+1,J+1,K} \\ & + (1-\gamma_x)(1-\gamma_y)\gamma_z \times \psi_{I,J,K+1} + \gamma_x(1-\gamma_y)\gamma_z \times \psi_{I+1,J,K+1} \\ & + (1-\gamma_x)\gamma_y \times \gamma_z \times \psi_{I,J+1,K+1} + \gamma_x \times \gamma_y \times \gamma_z \times \psi_{I+1,J+1,K+1}\end{aligned} \tag{28}$$

where the function ψ corresponds to scalar variables and ψ_n is their extrapolated value at location (x_n, y_n, z_n) and time t from the knowledge of their values at the scalar grid points (x_I, y_J, z_K). The weights γ_x, γ_y and γ_z vary between zero and unity and are defined as

$$\gamma_x = \frac{(x_n - x_I)}{(x_{I+1} - x_I)}, \quad \gamma_y = \frac{(y_n - y_J)}{(y_{J+1} - y_J)} \quad \text{and} \quad \gamma_z = \frac{(z_n - z_K)}{(z_{K+1} - z_K)} \tag{29}$$

5. The co-ordinates (x_n, y_n, z_n) of the particle at time t are recomputed using the interpolated values of the liquid velocity components [obtained at Step 3], while the relative particle velocity w_r is computed from Equation (8) using the particle radius r_n and the thermophysical properties of the liquid interpolated at location (x_n, y_n, z_n) and time t [obtained at Step 4],

$$x_n = x_a - u_{\infty,n}\Delta t \tag{30}$$

$$y_n = y_b - v_{\infty,n}\Delta t \tag{31}$$

$$z_n = z_c - (w_{\infty,n} + w_{r,n})\Delta t \tag{32}$$

$$\text{with} \quad w_{r,n} = \frac{2}{9}\frac{\rho_\infty g r_n^2}{\mu_{\infty,n}} \tag{33}$$

6. The ordinary differential equations for the particle internal co-ordinates $[r, (p_i)_{(1 \leqslant i \leqslant l)}]$ and for the density function f_1 [Equations (16)–(18)] at location (x_a, y_b, z_c) and time $t + \Delta t$ can then be integrated by the fourth order Runge–Kutta method [25].
7. Steps 2–6 are repeated until the difference between two successive computed values of x_n, y_n and z_n is less than an arbitrary value ε_1, i.e.

$$\text{Max}[|x_n(\text{iter}+1) - x_n(\text{iter})|, |y_n(\text{iter}+1) - y_n(\text{iter})|, |z_n(\text{iter}+1) - z_n(\text{iter})|] \leqslant \varepsilon_1 \tag{34}$$

where iter is the iteration step number. A sensitivity study has been performed and showed that the numerical solution was independent of ε_1 provided that it is less than 1.0×10^{-4} m.

8. Steps 1–7 are repeated for all interior points (x_a, y_b, z_c).
9. For steady state calculations, steps 1–8 are repeated until the maximum relative difference in the predictions of the particle internal co-ordinates $[r, (p_i)_{1 \leqslant i \leqslant l}]$ and of the density function f_1 between two successive iterations fall under an arbitrary constant ε_2:

$$\max_{\substack{2 \leqslant i \leqslant l_1 - 1 \\ 2 \leqslant j \leqslant m_1 - 1 \\ 2 \leqslant k \leqslant n_1 - 1}} \left[\frac{|X(\text{iter}+1) - X(\text{iter})|}{X(\text{iter})|} \right] \leqslant \varepsilon_2 \tag{35}$$

where X represents the internal co-ordinates r, $(p_i)_{1 \leqslant i \leqslant l}$ and f_1.

10. Steps 1–9 are repeated for all the points on the initial particle density function $f_{1,0}(r, (p_i)_{1 \leqslant i \leqslant l}, t)$.

3.2. Boundary point unit processes

The initial density function at the inlet boundary $f_{1,0}$ is determined from physical considerations or based on experimental data. The exit points are treated as interior points and the same procedure as that previously described is followed. Finally, Dirichlet, Neuman or mixed boundary conditions can be applied at the solid boundary points. In the present work, the weak boundary conditions were assumed for r, f_1 and p_i at the walls.

The advantage of the proposed method is that even the most complicated problem may be solved with relative ease. As the complexity of the problem increases, the complexity of the formulation and the solution effort increase much more rapidly for conventional techniques. Therefore, the modified method of characteristics will be preferable for problems beyond a certain complexity. For example, the present method is recommended for multidimensional problems with complex flow pattern where the density function depends on the external fields. In addition, the method is compatible and can be used in combination with other numerical schemes (e.g. finite-volume, finite elements) that may be used to compute the external variables.

4. COMPUTER PROGRAM VALIDATION

A set of test problems was chosen in order to compare the numerical predictions against practical problems whose analytical solutions are known and can be summarized as follows:

1. Solid particle in one-dimensional laminar flow—transient and steady-state situations.
2. Bubble or droplet transport and growth in one-dimensional vertical laminar flow.

In all the cases considered for validation, the liquid temperature, the liquid viscosity and density are assumed to be uniform and constant with time over the entire computational domain and the coupling between the particles and the external fields is not accounted for, i.e. the variables Y_j are constant. Even though the flow considered are one-dimensional (i.e. $u_\infty = v_\infty = 0$) the calculations were performed for a three-dimensional computational domain. The container is taken to be a parallelepiped of height, length and width denoted by H, L and W, respectively.

4.1. Solid particles in one-dimensional laminar flow

For validation purposes, we consider the physical situation when monodispersed solid particles of constant radius r are injected at the bottom of a vertical container. The liquid under one-dimensional laminar flow conditions with a uniform and constant upward velocity of 0.2 m/s, i.e. $\mathbf{v}_\infty = w_\infty \mathbf{k} = 0.2\mathbf{k}$, is considered. The particles are subject to buoyancy and are assumed to be small and in low concentration so that their presence does not affect the liquid flow. Then, the population balance equation simplifies to

$$\frac{\partial f_1}{\partial t} + (w_\infty + w_r)\frac{\partial f_1}{\partial z} = 0 \tag{36}$$

4.1.1. Transient situation. In this example, the particles are injected uniformly across the bottom of the container (at $z = 0$) and the injection rate varies with time so that the particle

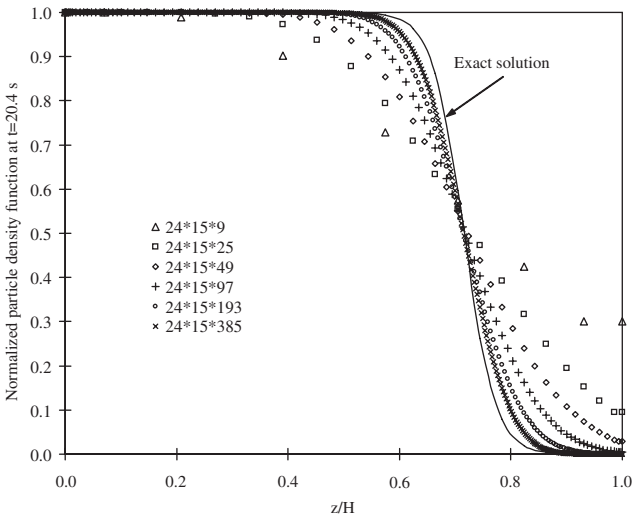

Figure 6. Comparison between the predictions of the method of characteristics and the analytical solution for solid particle density function under one-dimensional transient flow at time $t = 20.4$ s.

density function at $z = 0$ and time t is denoted $F(t)$. In the present study we assume that the particle density function at the bottom of the column varies with time according to the following Fermi function,

$$f_1(z=0,t) = F(t) = f_0 \left[\frac{e^{a(t-t_0)}}{1 + e^{a(t-t_0)}} \right] \tag{37}$$

where a, t_0 and f_0 are arbitrary constants. Thus, the transient particle density function at time t and location z solution of Equation (36) is given by

$$f_1(z,t) = F(u) \quad \text{where } u = t + z/(w_\infty + w_r) \tag{38}$$

i.e.

$$f_1(z,t) = \left\{ \frac{e^{a[t+z/(w_\infty+w_r)^{-t_0}]}}{1 - e^{a[t+z/(w_\infty+w_r)-t_0]}} \right\} f_0 \tag{39}$$

The numerical calculations were performed with the particle radius and the fluid properties such that the fluid flow is laminar and that the particle upward velocity $(w_\infty + w_r)$ is equal to 4 cm/s while the parameters at the particle injection cross-section (i.e. at $z = 0$) are $a = 1.4\,\text{s}^{-1}$, $t_0 = 2$ s and $f_0 = 10^5/\text{m}^3$ of liquid/m. Figure 6 shows a comparison of the particle density function using dimensionless variables along the z-axis at time $t = 20.4$ s obtained numerically with the exact solution. One can see that as the grid size is refined, the predictions of the numerical model converge toward the exact solution [Equation (38)]. The rapid changes in the particle injection rate with time forces one to reduce the grid size significantly in order to capture the sharp variation of the injection rate.

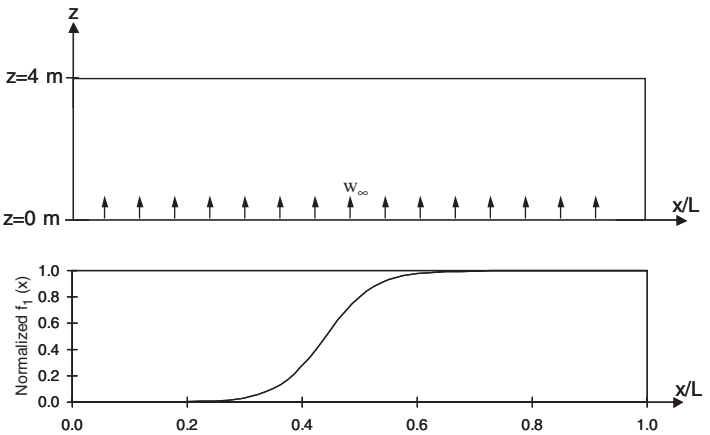

Figure 7. Schematic of the two-dimensional computational domain used for simulating steady-state transport of solid particles in two-dimensional laminar flow.

4.1.2. Steady-state situation. Here, the particles are not injected uniformly at the bottom of the container, instead the particle density function at $z = 0$ varies in the x-direction, i.e. $f_1(x, y, 0, r, t) = G(x)$ as illustrated in Figure 7. Then, under steady-state conditions, the particle density function at any location z should be the same as that at the bottom of the container, i.e.

$$f_1(x, y, z, r) = G(x) \tag{40}$$

Figure 8 illustrates a comparison of the numerical results with the analytical solution for the particular example when

$$G(x) = \left[\frac{e^{a(x-x_0)}}{1 + e^{a(x-x_0)}}\right] f_0 \tag{41}$$

with the parameters $a = 1.5\,\mathrm{m}^{-1}$, $x_0 = 0.7\,\mathrm{m}$ and $L = 1\,\mathrm{m}$. The tank was discretized in Cartesian co-ordinates using a $24 \times 15 \times 9$ grid. All the particles were assumed to be 1 mm in radius. Very good agreement exists between the numerical and the analytical solutions even with a coarse grid.

A monodispersed particle distribution has been chosen for illustrative purposes but similar results can be obtained for any arbitrary polydispersed population of solid particles. It suffices only to perform the same calculation for different radii and the corresponding values of the particle density function.

In conclusion, for solid particles transport in a one-dimensional vertical flows, the numerical scheme based on the modified method of characteristics yields results which are in very good agreement with theoretical solutions for both transient and steady-state conditions.

4.2. Bubbles rise at constant growth rate

This section is limited to bubble transport in steady-state one-dimensional laminar flow with constant particle growth rate $\dot{r}$ as shown in Figure 9. The population balance equation to be

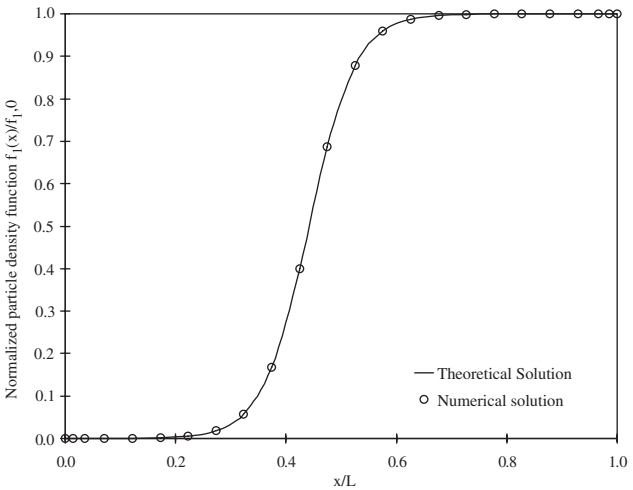

Figure 8. Comparison between the numerical solutions and the analytical solution for bubble density function under one-dimensional steady-state flow.

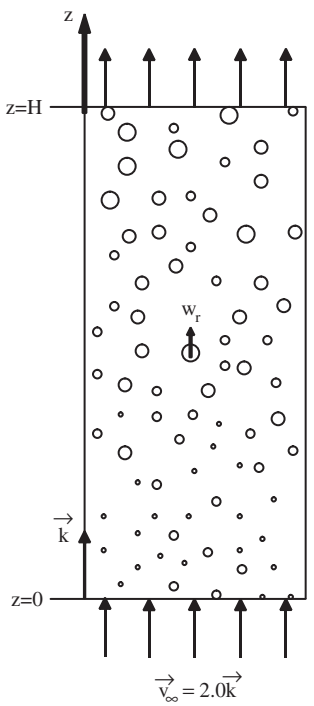

Figure 9. Schematic of a rectangular vertical container used for the code validation.

solved is written as

$$\frac{\partial}{\partial z}\left[(w_\infty + w_r) f_1\right] + \frac{\partial}{\partial r}\left(\dot{r} f_1\right) = 0 \tag{42}$$

where w_r is given by Equation (8). The liquid upward velocity is assumed to be $w_\infty = 0.2\,\mathrm{m/s}$ and the growth rate is taken as constant and equal to $\dot{r} = \dot{r}_0 = 1.0 \times 10^{-5}\,\mathrm{m/s}$. The governing equations to be solved simplify to

$$\frac{\mathrm{d}z}{\mathrm{d}t} = w_\infty(z) + w_r(r,z) \tag{43}$$

$$\frac{\mathrm{d}r}{\mathrm{d}t} = \dot{r}_0 \tag{44}$$

$$\frac{\mathrm{d}f_1}{\mathrm{d}t} = -f_1 \frac{\partial w_r(r,z)}{\partial z} \tag{45}$$

The bubble density function at the injection cross-section $z = 0$ is assumed to follow a normal distribution, i.e.

$$f_1(r, z=0, t) = \frac{1}{\sigma_0\sqrt{2\pi}} \exp\left[-\frac{(r-\mu_0)^2}{2\sigma_0^2}\right] \tag{46}$$

with a mean value $\mu_0 = 1$ mm and a deviation $\sigma_0 = 0.25$ mm.

In this specific case, an analytical solution to the population balance equation can be found if one recognizes that the bubbles are small and their relative velocity with respect to the liquid w_r is negligible compared with the velocity of the liquid ($w_r \ll w_\infty$). In other words, the bubble density function $f_1(z,r)$ shifts toward larger r in the r-space when bubbles are transported from location $z = 0$ m to $z = H$ m, i.e. a bubble entering the column at $z = 0$ with a radius r reaches the location z with a radius $r + \dot{r}_0 z/w_\infty$. Then, the bubble density function f_1 at location z is given by

$$f_1(z,r) = \frac{1}{\sigma_0\sqrt{2\pi}} \exp\left\{-\frac{[(r - \dot{r}_0 z/w_\infty) - \mu_0]^2}{2\sigma_0^2}\right\} \tag{47}$$

Figure 10 compares the bubble density function at locations $z = 0$ m obtained numerically with the analytical solution given by Equation (47). The results clearly indicate that the numerical model agrees very well with the exact solution. Note also that extension of this example to droplet transport and evaporation in one-dimensional gas flow is straightforward.

4.3. Bubbles transport and growth due to pressure changes

In this section, the gas bubbles are transported with the upward flowing liquid and by buoyancy while they can grow due the change in hydrostatic pressure as shown in Figure 9. The pressure drop in the liquid phase is neglected and the pressure at $z = 0$ m is assumed to equal the atmospheric pressure p_0. The following equations are to be solved by the modified method

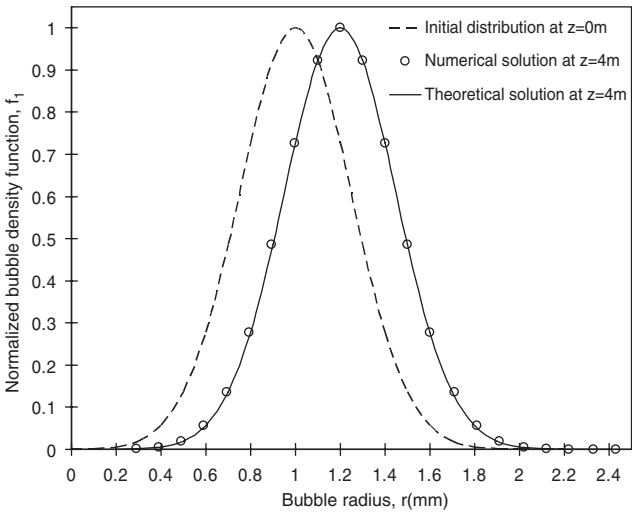

Figure 10. Comparison between the numerical solution and the analytical solution for bubble rise at constant growth rate ($\dot{r} = 0.01$ mm/s) under one-dimensional steady-state flow at $z = 4$ m with $\mu_0 = 1$ mm, $\sigma_0 = 0.25$ mm, $\mathbf{w}_\infty = 0.2\mathbf{k}$ m/s.

of characteristics,

$$\frac{\mathrm{d}z}{\mathrm{d}t} = w_\infty(z) + w_r(r,z) \tag{48}$$

$$\frac{\mathrm{d}r}{\mathrm{d}t} = \dot{r}(r,z) \tag{49}$$

$$\frac{\mathrm{d}f_1}{\mathrm{d}t} = -f_1\left[\frac{\partial w_r(r,z)}{\partial z} + \frac{\partial \dot{r}(r,z)}{\partial r}\right] \tag{50}$$

where w_r and its derivative with respect to z are given by Equations (8) and (19), respectively. The bubble growth rate $\dot{r}$ and its derivative with respect to bubble radius are expressed as

$$\dot{r} = \frac{\rho_\infty g(w_\infty + w_r)r/3}{p_0 + \rho_\infty g z + 4\sigma/3r} \tag{51}$$

$$\frac{\partial \dot{r}}{\partial r} = \frac{\rho_\infty g}{3}\left[\frac{(w_\infty + 3w_r)}{p_0 + \rho_\infty g z + 4\sigma/3r}\right] + \frac{4\sigma}{3r^2}\left[\frac{\dot{r}}{p_0 + \rho_\infty g z + 4\sigma/3r}\right] \tag{52}$$

Here, the liquid density, viscosity and surface tension correspond to those of soda-lime silicate glass at 1800 K and are equal to 2406 kg/m^3, 5.53 Pa s and 296 mN/m, respectively. The initial bubble density function is assumed to follow a normal distribution [Equation (46)] with a mean value of $\mu_0 = 1$ mm and a deviation $\sigma_0 = 0.25$ mm.

4.3.1. Bubble rise dominated by the upward liquid flow. In the present example, the relative velocity of the bubble with respect to the liquid w_r can be neglected compared with the liquid velocity w_∞. Its partial derivative with respect to z is also negligible in comparison with that of $\dot{r}$ with respect to the bubble radius r. Moreover, the term due to surface tension in the denominator is assumed to be negligible, i.e. $4\sigma/3r \ll (p_0 + \rho_\infty gz)$. This assumption is valid for bubble radii larger than 0.2 mm. Note that, if the liquid flows upward ($w_\infty > 0$), the bubbles grow and the growth rate $\mathrm{d}r/\mathrm{d}t$ is positive. The approximate solution to the problem of interest can be written as

$$z(t) = w_\infty t \tag{53}$$

$$r(t) = r_0 \left(\frac{p_0 + \rho_\infty gz}{p_0} \right)^{1/3} \tag{54}$$

$$f_1(r) = f_1(r_0) \left(\frac{r_0}{r} \right) \tag{55}$$

where r_0 is the bubble radius at location $z = 0$ m at time $t = 0$ s. Note that the approximate analytical solution satisfies the conservation of the same total number of bubbles N,

$$N(z) = \int_0^\infty f_1(r)\,\mathrm{d}r = \int_0^\infty f_1(r_0)\frac{r_0}{r}\,\mathrm{d}r = \int_0^\infty f_1(r_0)\,\mathrm{d}r_0 = N(z=0) \tag{56}$$

Figure 11 illustrates a comparison of the approximate analytical solution given by Equation (55) with the numerical results for Equations (50)–(52). The numerical solutions

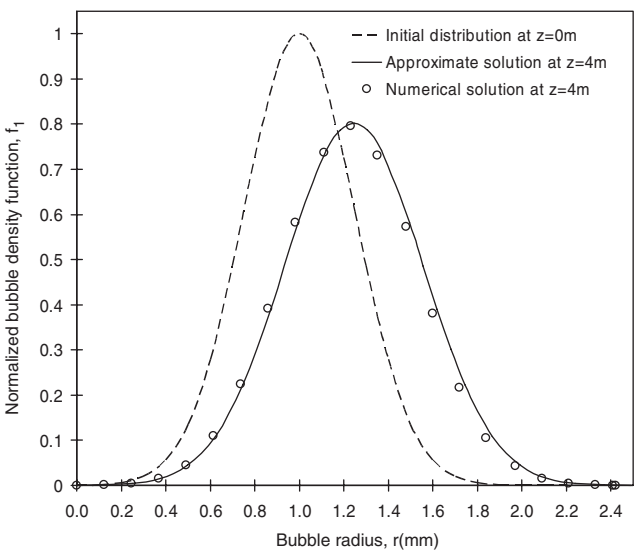

Figure 11. Comparison between the method of characteristics and the approximate analytical solution for bubble rise and growth due to pressure change under one-dimensional steady-state flow with $\mu_0 = 1$ mm, $\sigma_0 = 0.25$ mm, $\mathbf{w}_\infty = 0.2\mathbf{k}$ m/s.

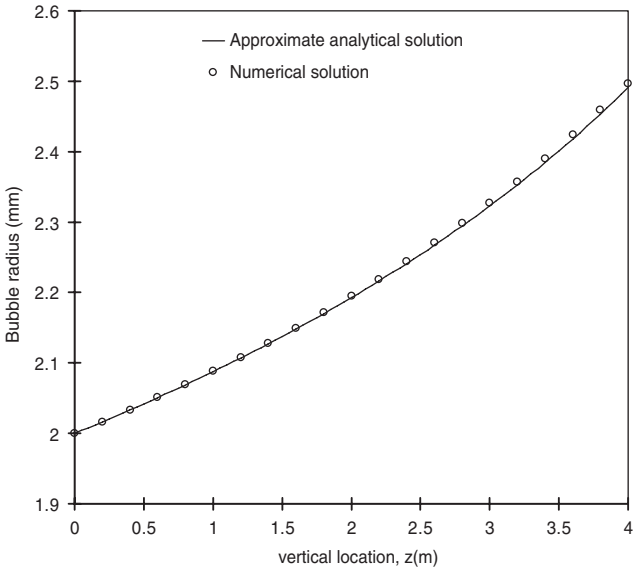

Figure 12. Comparison between the method of characteristics and the approximate analytical solution [Equation (54)] for the profile of bubble radius $r(z)$ as a function of z with $r_0 = 2\,\text{mm}$ at $z = 0\,\text{m}$ and $\mathbf{w}_\infty = 0.2\mathbf{k}\,\text{m/s}$.

compare very well with the approximate analytical solution. The slight discrepancies may be explained by the approximation made to solve the problem analytically that tend to underestimate the bubble growth. One can see that unlike the results for constant growth rate, the bubble density function at the top of the column ($z = 4\,\text{m}$) is not symmetric around the mean value due to the fact that the growth rate increases linearly with the bubble radius as given by Equation (51) when w_r is negligible compared with w_∞, i.e. the large bubbles grow faster than the smaller ones. Finally, the variation of the bubble radius $r(z)$ and the bubble density function $f_1(r,z)$ with the vertical location z for an initial bubble radius $r_0 = 2\,\text{mm}$ at $z = 0\,\text{m}$ is shown in Figures 12 and 13, respectively. Again, good agreement between the approximate analytical and the numerical solution is observed.

4.3.2. Bubble rise dominated by buoyancy. Here, the gas bubbles rise by buoyancy only, i.e. $w_\infty = 0\,\text{m/s}$ and can grow due the changes in the hydrostatic pressure. Similarly, assuming that the term due to surface tension in the denominator is negligible compared with the hydrostatic pressure, i.e. $4\sigma/3r \ll (p_0 + \rho_\infty gz)$, an analytical solution can be found for the radius r and the bubble density function f_1 at every location z in the column are given by

$$r(z) = r_0 \left(\frac{p_0 + \rho_\infty gz}{p_0} \right)^{1/3} \tag{57}$$

$$f_1(z) = f_1(r_0) \left(\frac{r_0}{r} \right)^5 \tag{58}$$

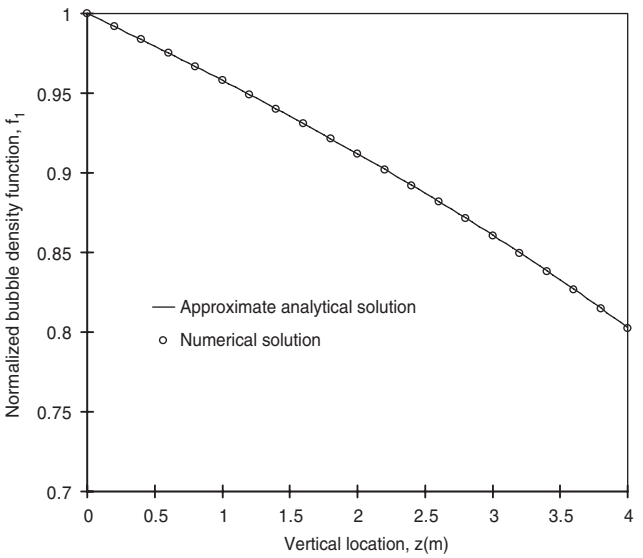

Figure 13. Comparison between the method of characteristics and the approximate analytical solution [Equation (55)] for the profile of bubble density function $f_1(z)$ as a function of z with $r_0 = 2$ mm at $z = 0$ m and $\mathbf{w}_\infty = 0.2\mathbf{k}$ m/s.

where r_0 and $f_1(r_0)$ are the bubble radius and the bubble size distribution at location $z = 0$ m, respectively.

Figure 14 shows a comparison of the approximate analytical solution given by Equation (58) and the numerical results. The latter are in very good agreement with the approximate analytical solution. Note that the variations of the bubble radius $r(z)$ with the vertical location z for an initial bubble radius $r_0 = 2$ mm at $z = 0$ m are the same as those when the bubble rise is dominated by the upward liquid flow (see Figure 12) and need not be repeated. The bubble density function $f_1(r,z)$ with the vertical location z for an initial bubble radius $r_0 = 2$ mm at $z = 0$ m is shown in Figure 15. Excellent agreement between the approximate analytical solution and the numerical solution is evident. Note that in the present case, the total number of bubbles is not conserved, i.e. $\int_0^\infty f_1(r)\,\mathrm{d}r \neq \int_0^\infty f_1(r_0)\,\mathrm{d}r_0$. This is due to the fact that the gas and liquid momentum equations have been decoupled and it was assumed that the vertical component of the bubble velocity vector was given by $w_b = w_\infty + w_r$. Thus, this assumption implies that the bubble velocity field does not satisfy the steady-state continuity equation, i.e. $\nabla \cdot \mathbf{v}_b \neq 0$. Therefore, the conservation of the total number of bubbles cannot be assured. For example, in the case of convective transport of solid particles without generation and growth, the conservation equation [Equation (36)] along the pathlines of the particles may be written as $\mathrm{d}f_1/\mathrm{d}t = f_1 \partial w_r/\partial z$. However, physically it is clear that the bubble density function is transported unchanged along the particle pathlines and the conservation equation can be written as $\mathrm{d}f_1/\mathrm{d}t = 0$. Therefore, the assumption on the bubble velocity introduces an artificial source in the population balance equation. In order to approximately conserve the total number of bubbles the bubble velocity vector should satisfy

$$\nabla \cdot \mathbf{v}_b \approx 0 \tag{59}$$

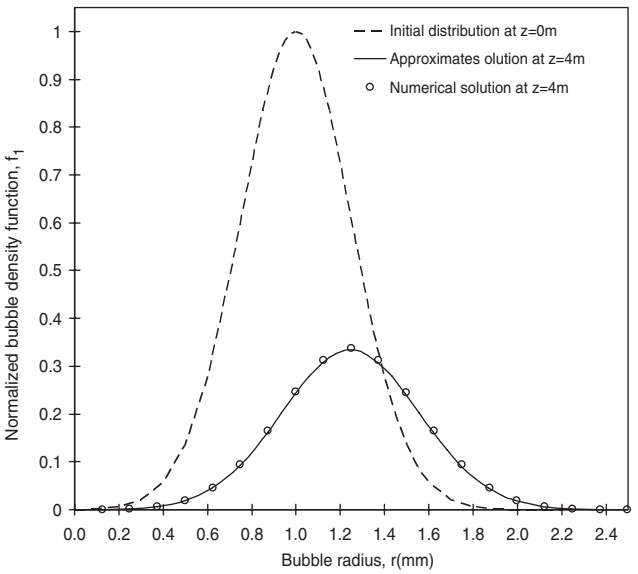

Figure 14. Comparison between the method of characteristics and the approximate analytical solution for bubble rise due to buoyancy and growth due to pressure change under one-dimensional steady-state flow with $\mu_0 = 1$ mm, $\sigma_0 = 0.25$ mm, $\mathbf{w}_\infty = 0.0\mathbf{k}$ m/s.

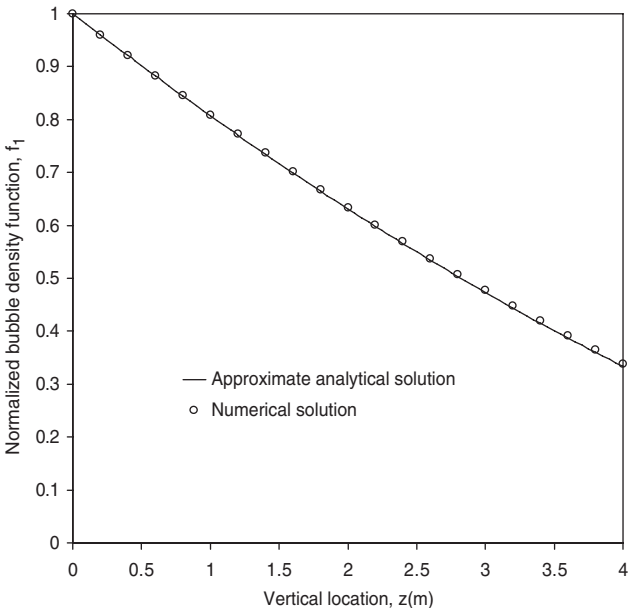

Figure 15. Comparison between the method of characteristics and the approximate analytical solution [Equation (58)] for the profile of bubble density function f_1 as a function of vertical location—one-dimensional steady-state flow with $r_0 = 2$ mm at $z = 0$ m and $\mathbf{w}_\infty = 0.0\mathbf{k}$ m/s.

Since the liquid is treated as incompressible, Equation (59) is satisfied if $\partial w_r/\partial z \ll 1$. Physically, this corresponds to situation when the bubble growth rate and liquid velocity do not vary significantly with position and time. This problem does not occur either in the case of bubble growth and rise dominated by the liquid flow since $\nabla \cdot \mathbf{v}_b \approx \nabla \cdot \mathbf{v}_\infty \approx 0$ or for solid particle rise by buoyancy without growth since then $\partial w_r/\partial z = 0$. However, for bubble rise dominated by buoyancy, the simplifying assumption $w_b = w_\infty + w_r$ must be relaxed and the coupling between the bubble rise and the liquid flow should be accounted for. To do so, one could couple the mass and momentum conservation equations for both phases using the two-fluid model [1, 2]. However, this task is complicated and beyond the scope of this study.

In conclusion, the results reported in this section validate the numerical computer program. Previous examples have analytical solutions and could have been solved using the conventional method of characteristics (direct marching method) since they were concerned with one-dimensional flow and with bubbles having one internal co-ordinate (their radius r). The numerical results obtained compare well with the analytical solution and validate the numerical scheme.

5. CONCLUSION

This paper has described in detail a new numerical method for solving the population balance equation using the modified method of characteristics. The numerical solution has been compared with the analytical solution for simple one-dimensional flow cases when it was possible. Very good agreement between the numerical and the theoretical solutions has been obtained confirming the validity of the numerical procedure and the associated computer program.

The modified method of characteristics enables one to solve the population balance equation for complicated problems with relative ease while conventional techniques become rapidly complex or inadequate. In addition, the method is compatible and can be used in combination with other numerical schemes (e.g. finite-volume, finite elements) that may be used to compute the external variables. For example, the numerical scheme developed in the present study could easily be coupled to the three-dimensional two-fluid model to solve for polydispersed bubble size distribution and could be applied, for example, to two-phase flow around a naval surface ship [3].

Finally, since computations for each point on the initial bubble density function $f_{1,0}$ are independent from one another, parallel computing is highly recommended to significantly reduce the computational time. Moreover, the local particle density function and the conditions in the surrounding liquid phase (temperature, velocity vector, gas concentration) are interdependent. Accounting for the coupling between the particle density function and the external fields is straightforward but time consuming. Indeed, accounting for the coupling requires iteratively solving for the external fields and then for the population balance equation until the convergence criteria are met. However, such a procedure falls beyond the scope of this study and has been disregarded for the sake of clarity as the authors wanted to emphasize on the modified method of characteristics. Applications to bubble transport and growth/shrinkage in three-dimensional flow will be reported shortly.

NOMENCLATURE

f_1	particle density function
g	specific gravity
h	particle net generation rate per unit volume in the state space
H	height of the column
$\mathbf{i}, \mathbf{j}, \mathbf{k}$	unit vectors in the physical space
l	number of internal co-ordinates other than the particle radius
m	number of variables in external fields
N	total number of particles
p_i	particle internal co-ordinates other than radius ($1 \leqslant i \leqslant l$)
p	pressure
r	particle or bubble radius
$\dot{r}$	time rate of change of particle or bubble radius
R	universal gas constant $= 8.314\ \mathrm{J/mol\,K}$
$\mathbf{S}$	particle state vector
t	time
u	projection of the velocity vector on the x-axis
v	projection of the velocity vector on the y-axis
$\mathbf{v}$	velocity vector
w	projection of the velocity vector on the z-axis
w_r	vertical upward velocity of the particle relative to the glass melt
$\mathbf{x}$	spatial or external co-ordinates
x	longitudinal location
y	spanwise location
Y	local continuous phase variables
z	vertical location oriented upward

Greek symbols

α	arbitrary constant with values between 0 and 1
$\beta_{u,v,w}$	weighting parameters for Laplacian interpolation for the vector variables
$\gamma_{x,y,z}$	weighting parameters for Laplacian interpolation for the scalar variables
ε	arbitrary small constant for numerical converge criteria
σ	surface tension
σ_0	standard deviation of the particle density function
ρ	density
μ	kinematic viscosity
μ_0	mean value of the particle density function
$\mu_m^{(i)}$	sectional moment of the density function of order m [Equation (2)]
μ_m	total moment of the bubble density function of order m [Equation (2)]

Subscripts

0	refers to initial values
b	refers to the particles or bubbles

i, j, k indices for the vector nodes of a staggered grid (see Figure 1)
I, J, K indices for the scalar nodes of a staggered grid (see Figure 1)
i index of the internal variable
n index of the particle group
∞ refers to the bulk of the liquid phase

Notation

$\dot{X}$ derivative of property X with respect to time

ACKNOWLEDGEMENTS

This work was supported in part by the U.S. Department of Energy/Glass Industry/Argonne National Laboratory/University collaborative research project. The authors are indebted to Prof. D. Ramkrishna from the Chemical Engineering Department at Purdue University for his helpful discussions and constructive comments.

REFERENCES

1. Ishii M. *Thermo-Fluid Dynamics Theory of Two-Phase Flow*. Eyrolles: Paris, 1975.
2. Lahey RT, Drew DA. On the development of multidimensional two-fluid models for vapor/liquid two-phase flows. *Chemical Engineering Communications* 1992; **118**:125–139.
3. Carrica PM, Bonetto FJ, Drew DA, Lahey Jr RT. The interaction of background ocean air bubbles with a surface ship. *International Journal for Numerical Methods in Fluids* 1998; **28**:571–600.
4. Ramkrishna D. The status of population balances. *Review in Chemical Engineering* 1985; **3**(1):49–95.
5. Ramkrishna D. *Population Balances*. Academic Press: San Diego, CA, 2000.
6. Motz S, Mitrović A, Gilles E-D. Comparison of numerical methods for the simulation of dispersed phase systems. *Chemical Engineering Science* 2002; **57**:4329–4344.
7. Kumar S, Ramkrishna D. On the solution of population balance equation by discretization—I a fixed pivot technique. *Chemical Engineering Science* 1996; **51**(8):1311–1332.
8. Kumar S, Ramkrishna D. On the solution of population balance equation by discretization—II a moving pivot technique. *Chemical Engineering Science* 1996; **51**(8):1311–1332.
9. Kumar S, Ramkrishna D. On the solution of population balance equation by discretization—III nucleation, growth, and aggregation of particles. *Chemical Engineering Science* 1997; **52**(4):4659–4679.
10. Ungan A, Payli RU, Balkanli B. Numerical model of polydispersed silica grain dissolution in glass melting furnaces. *Journal of the American Ceramic Society* 1994; **77**(7):1921–1927.
11. Balkanli B, Ungan A. Numerical simulation of bubble behaviour in glass melting tanks. Part 4. Bubble number density distribution. *Glass Technology* 1996; **3**(5):164–168.
12. Rousseaux J-M, Vial C, Muhr H, Plasari E. CFD simulation of precipitation in the sliding-surface mixing device. *Chemical Engineering Science* 2001; **56**:1677–1685.
13. Hounslow MJ, Ryall RL, Marshall VR. A discretized population balance for nucleation, growth, and aggregation. *AIChE Journal* 1988; **34**(11):1821–1832.
14. Allievi A, Bermejo R. Finite element modified method of characteristics for Navier–Stokes equations. *International Journal for Numerical Methods in Fluids* 2000; **32**:439–464.
15. Patankar S. *Numerical Heat Transfer and Fluid Flow*. Hemisphere: Washington, DC, 1980.
16. Marcum DL, Hoffman JD. Calculation of three-dimensional flowfields by the unsteady method of characteristics. *AIAA Journal* 1985; **23**(10):1497–1505.
17. Marcum DL. Calculation of three-dimensional inviscid flowfields. *Ph.D. Thesis*, Purdue University, 1985.
18. Wang BN, Hoffman JD. Calculation of annular nozzle trisonic flowfields by the method of characteristics. *Journal of Propulsion and Power* 1988; **4**(3):228–235.
19. Parpia IH. Multidimensional time dependent method of characteristics. *Ph.D. Thesis*, Purdue University, 1986.
20. Dabral MM, Roy S, Bhaskarwar AN. General kinetic invariant model of dissolution of large polydisperse particles. *The Chemical Engineering Journal* 1996; **61**:161–170.
21. Hunter JB, Asenjo JA. A population balance model of enzymatic lysis of microbial cells. *Biotechnology and Bioengineering* 1990; **35**:31–42.

22. Shah BH, Ramkrishna D. A population balance model for mass transfer in lean liquid–liquid dispersion. *Chemical Engineering Science* 1973; **28**:389–399.
23. Magnaudet JJM. The forces acting on bubbles and rigid particles. In *ASME Fluids Engineering Division Summer Meeting*, *FEDSM'97*, *Part 16*, Vancouver, Canada, June 22–26, 1997.
24. Fox RW, McDonald AT. *Introduction to Fluid Mechanics* (5th edn). Wiley: New York, NY, 1998.
25. Hoffman JD. *Numerical Methods for Engineers and Scientists*. McGraw Hill: New York, NY, 1998.

